



Degree Project in Computational Mathematics

Second cycle, 30 credits

Modeling and Simulation of the Pneumatic System of an Intra-Aortic Balloon Pump

ELLEN MATTSSON

Modeling and Simulation of the Pneumatic System of an Intra-Aortic Balloon Pump

ELLEN MATTSSON

Master's Programme, Applied and Computational Mathematics, 120 credits
Date: September 19, 2025

Supervisors: Kenny Rumindo, Jennifer Ryan
Examiner: Jennifer Ryan

Host company: Getinge AB
Swedish title: Modellering och simulering av det pneumatiska systemet i en
aortaballongpump

Abstract

Cardiovascular disease is the leading cause of death globally, and mechanical circulatory support devices such as the intra-aortic balloon pump (IABP) play a vital role in treatment in acute care. This thesis develops and validates a lumped-parameter Simscape model of the pneumatic system in Getinge's CardioSave IABP. The model incorporates conservation of mass, momentum and energy for compressible gas flow, and includes the compressor, safety disk (SD), tubing, and balloon. Three balloon representations were compared: (i) linear spring-damper, (ii) nonlinear spring-damper, and (iii) a soft spring with check valves to capture inflation and deflation thresholds. Parameters were estimated using least-squares optimization and the model was validated against experiments using a 40 cc balloon under external pressures of 25, 50 and 100 mmHg (gauge). The check valve model best reproduced the observed threshold behavior and achieved the lowest average shuttle pressure error. A use case study across atmospheric pressures of 450-760 mmHg and heart rates 30-200 bpm showed 10-90 % inflation and deflation times ≤ 0.12 s, with full inflation volumes within acceptance limits. The index-1 DAE system was solved with an NDF2-based implicit solver, yielding stable and efficient simulations with small dispersive errors. While the simplified compressor model does not capture measured LPM-RPM curves across altitudes, the system-level dynamics are reproduced, making it useful for evaluating control strategies and design verification.

Sammanfattning

Hjärt- och kärlsjukdomar är den ledande dödsorsaken globalt, och mekaniska cirkulationsstöd som intra-aortisk ballongpump (IABP) spelar en viktig roll vid akutvård. I detta examensarbete utvecklas och valideras en matematisk modell av det pneumatiska systemet i Getinges CardioSave IABP, implementerad i Simscape. Modellen bygger på lagar om bevarande av massa, rörelsemängd och energi för kompressibelt flöde och inkluderar kompressor, 'safety disk' (SD), slangsystem samt ballong. Tre olika ballongrepresentationer jämfördes: (i) linjärt fjäder-dämpare-system, (ii) icke-linjärt fjäder-dämpare-system samt (iii) en mjuk fjäder med backventiler för att beskriva tryck-trösklar vid uppblåsning och tömning. Parametrar identifierades med minsta kvadrat-metoden och modellen validerades mot experiment med en 40 cc-ballong under yttre tryck på 25, 50 och 100 mmHg (gauge). Backventilmodellen återgav bäst de observerade tröskelbeteendena och gav lägst genomsnittligt fel. En användningsstudie vid atmosfäriskt tryck mellan 450-760 mmHg och hjärtfrekvenser mellan 30-200 slag per minut visade 10-90 % uppblåsnings- och tömningstider ≤ 0.12 s samt full uppblåsningsvolym inom acceptansgränserna. Det skapade index-1 DAE-systemet löstes med en implicit NDF2-baserad numerisk metod, vilket gav stabila och effektiva simuleringar med mindre dispersiva effekter. Även om den förenklade kompressormodellen inte återger uppmätta LPM-RPM-kurvor, lyckas modellen reproducera dynamiken på systemnivå, vilket gör att modellen är användbar för utvärdering av nya strategier och verifiering.

Acknowledgments

I would like to thank my supervisor at Getinge, Kenny Rumindo, for his guidance, support, and encouragement throughout this thesis work. I would also like to thank my academic supervisor at KTH, Jennifer Ryan, for her continuous support, patience, and constructive feedback during this project.

I also want to extend my gratitude to the entire research team at Getinge for their warm welcome and for sharing their time, insights, and expertise in the medtech field.

Contents

1	Introduction	1
1.1	About the company	1
1.2	Problem definition	1
1.3	Aim and objectives	2
2	Background	3
2.1	The human heart	3
2.1.1	The cardiac cycle	3
2.1.2	Myocardial infarction	4
2.1.3	Congestive heart failure	4
2.2	Intra-aortic balloon pump (IABP)	5
2.2.1	Early development	5
2.2.2	Current practice	5
2.2.3	Pneumatic system overview	6
2.3	Literature review	7
2.3.1	IABP modeling techniques	7
2.3.2	Previous work	8
3	Mathematical model	9
3.1	Preliminaries	9
3.1.1	Ideal gas law	9
3.1.2	Compliance and stiffness	9
3.1.3	Pressure loss	10
3.2	Drive side	10
3.3	Tubing gas dynamics	11
3.3.1	Conservation of mass	12
3.3.2	Conservation of momentum	13
3.3.3	Conservation of energy	14
3.3.4	Pipe fittings and bending	15
3.4	Balloon subsystem	16
3.4.1	Spring-damper system	17
3.4.2	Valve threshold model for balloon dynamics	17
3.5	Model adjustments for resistance behavior	18
4	Method	20
4.1	Software	20
4.2	Differential-algebraic equations	20
4.3	Backward and numerical differentiation formulas	21
4.4	Simulation framework	22
4.4.1	Solver choice	23
4.5	Experimental work	23
4.5.1	Compressor characterization	23
4.5.2	Balloon inflation and validation tests	24
4.6	Parameter estimation	24
4.6.1	Case 1: Check-valve parameters	25

4.6.2	Case 2: Compressor variables	25
4.7	Use case: Altitude test	26
4.8	Modified equation analysis	27
5	Results	28
5.1	Drive side	28
5.2	Shuttle pressure (balloon subsystem results)	29
5.2.1	Comparison of balloon models	32
5.3	Use case results: Altitude test	34
6	Discussion	36
6.1	Compressor	36
6.2	Resistance	37
6.3	Balloon models	38
6.4	Valve dynamics	38
6.5	Parameter estimation	39
6.6	Numerical method	39
7	Conclusions and future Work	40
7.1	Conclusions	40
7.2	Future work	40
	References	41

1 Introduction

According to the World Health Organization (WHO), cardiovascular diseases are the leading cause of death globally, causing around 17.9 million deaths each year [31]. More than four out of five cardiovascular disease deaths are due to heart attacks and strokes. Among the cardiovascular conditions, myocardial infarction is the most common cause of mortality worldwide [21].

To help treat such life-threatening events, mechanical circulatory devices have been developed to treat patients with severe cardiac dysfunction. Among these, the intra-aortic balloon pump (IABP) has long been one of the most used devices [13]. The IABP uses counterpulsation, with the balloon inflating during diastole and deflating in systole, augmenting coronary perfusion and reducing left ventricular afterload. This helps support the heart in critical conditions.

1.1 About the company

Getinge is a MedTech company founded by Olander Larsson in 1904 in Getinge, Sweden. It began as a company for manufacturing agricultural equipment, but later began manufacturing sterilizers and disinfection solutions for medical use. Today, Getinge develops and distributes a range of advanced medical technologies, such as respirators, extracorporeal membrane oxygenation (ECMO) systems, and intra-aortic balloon pumps (IABPs) [1]. Their IABP on the market today is called CardioSave, and is the subject of this project.

The intra-aortic balloon pump (IABP) consists of a catheter, an intra-aortic balloon (IAB) and a console connected to the catheter. The IAB is a long balloon which is inserted into a patient's aorta. The console is responsible for the control and drive mechanisms that regulate the inflation and the deflation of the balloon in sync with the cardiac cycle.

1.2 Problem definition

In the development of medical devices, such as those intended for use in critical care, rigorous testing is essential to ensure safety and efficiency. However, physical prototyping and clinical simulations can be time-consuming and costly, especially in early-stage design or when evaluating small technical modifications. Therefore, a common and effective approach to face these challenges is the use of computational modeling and simulation tools, which can provide valuable insights into system behavior under various scenarios before committing to physical prototypes or clinical studies.

Currently, there is interest in a more accurate and flexible mathematical representation of the pneumatic system used in Getinge's intra-aortic balloon pump CardioSave. Many studies have examined the effects of IABP therapy in patient models, but to model the machine itself remains relatively rare. An existing model of the pneumatic system has previously been developed, with a functioning model of the inflation and deflation and a simplified pressure source to represent the console of the machine.

1.3 Aim and objectives

The primary aim of this project is to develop a more realistic and test-ready mathematical model of the pneumatic system within Getinge's intra-aortic balloon pump. This model aims to simulate the dynamic behavior of the inflation and deflation cycles under different operating conditions. The objectives for this thesis are:

- To analyze the structure and function of the pneumatic system in Getinge's IABP CardioSave, including valves, pressure sources and timing mechanisms.
- To extend the existing IABP model and validate it against experimental data.
- To evaluate the model's performance under various simulated conditions.

2 Background

2.1 The human heart

The heart consists of two separate pumps. The right side of the heart pumps deoxygenated blood through the lungs for oxygenation, while the left side receives the oxygenated blood from the lungs and ejects it to the rest of the body and peripheral organs through the aorta.

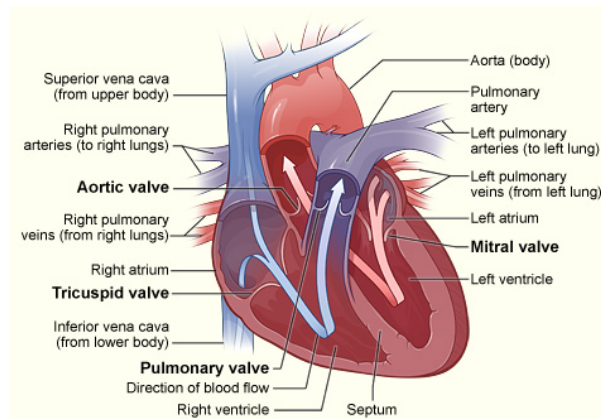


Figure 2.1: Cross-sectional view of the human heart. Image accessed from Wikimedia Commons [9].

Figure 2.1 shows a cross-sectional view of the human heart. The semilunar valves in the heart are the aortic valve and the pulmonary valve. The aortic valve is between the left ventricle and the aorta, while the pulmonary valve allows blood flow from the right ventricle to the pulmonary arteries, which carry oxygen-poor blood to the lungs. The aorta starts at the left ventricle, extending upwards in the body before bending downwards. The aorta descends from the heart, through the chest and abdominal cavities, and ends at the pelvis.

The femoral artery is a major blood vessel largely responsible for supplying oxygenated blood to the lower body [23]. It starts in the upper thigh near the groin and runs down to the back of the knee. The first part of the femoral artery is an extension of the external iliac artery in the pelvis [7].

2.1.1 The cardiac cycle

The events that occur from the beginning of a heartbeat to the beginning of the next are called the cardiac cycle. The cardiac cycle consists of a period of relaxation, diastole, where the heart is filled with blood, followed by a contraction phase called systole.

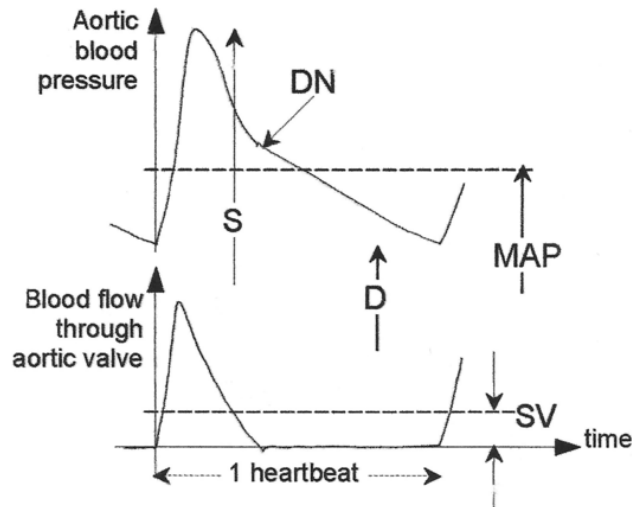


Figure 2.2: Aortic blood pressure and blood flow over the cardiac cycle. Image accessed from Wikimedia Commons [30].

When left ventricular ejection begins, the aortic valve opens which causes the pressure to rise in the aorta, reaching a peak before the pressure rapidly drops due to blood ejection [20]. The closure of the aortic valve marks a pressure event in the aortic pressure, marking the end of systole, and is visible in the aortic pressure as a slight rise in pressure followed by decreasing pressure until the next ventricular contraction. This slight pressure rise at the end of systole is called a dicrotic notch, which can be seen in Figure 2.2.

These pressure events are important concepts when it comes to the timing of inflation and deflation in the intra-aortic balloon pump.

2.1.2 Myocardial infarction

Myocardial infarction (MI), commonly referred to as "heart attack", is caused by complete or decreased stop of blood flow to a portion of the myocardium [18]. MI can either go undetected or it could be acute and lead to hemodynamic deterioration and sudden death. Coronary disease is the underlying cause to most myocardial infarctions. With coronary artery occlusion, the myocardium does not get oxygen in the affected part, with prolonged deprivation of oxygen to the myocardium possibly leading to myocardial cell death and necrosis.

2.1.3 Congestive heart failure

Congestive heart failure is a long-term condition that implies that the heart is unable to pump blood around the body properly. The heart can not handle the amount of blood that the body needs, causing blood to build up in other parts of the body, most commonly in the lungs, legs and feet [5]. The severity of the heart failure is mainly decided based on ejection fraction. Conditions that can lead to

heart failure include coronary heart disease and high blood pressure.

2.2 Intra-aortic balloon pump (IABP)

2.2.1 Early development

The possibility to alter timing of pressure events during a heartbeat were first introduced by Kantrowitz et. al [12]. Their tests showed a significant increase in diastolic pressure compared to previous control studies. Around the same time other researchers [19] experimented with counterpulsation, where they used femoral artery access to remove blood during systole and then replacing it in diastole. These experiments showed some hemodynamic impact but the technique was deemed impractical for clinical application and was not pursued. The first preliminary studies with an intra aortic balloon pump was made in 1961 by Mouloupoulos, Topaz, and Kolff [16], where a catheter in a long, narrow latex tube was inserted into the descending aorta of an anesthetized dog. This tube was then rhythmically inflated with carbon dioxide, inflating in diastole and deflating during systole. This study found that it was possible to increase the diastolic blood flow in the arterial system as well as lower the end diastolic arterial pressure. The first successful clinical treatment with an intra-aortic balloon pump (IABP) was reported in 1967 [19], where IABP therapy was successfully performed in a 45 year old female who had sustained a myocardial infarction and was comatose and in severe cardiogenic shock.

2.2.2 Current practice

An intra-aortic balloon pump (IABP) is a mechanical circulatory assist device in critically ill patients with cardiac disease. The intra-aortic balloon pump consists of a long, thin catheter with a balloon at the end, and a machine that controls the gas flow to and from the balloon. The balloon is most commonly inserted via the femoral artery, and the balloon tip should be positioned a bit distal to the left subclavian artery origin, which is confirmed via transoesophageal echocardiography or X-ray [11].

The balloon inflates when the aortic valve closes, at the dicrotic notch, displacing blood from the thoracic aorta into the peripheral circulation, followed by rapid deflation before the onset of systole. When the balloon inflates, this leads to a potential increase in coronary blood flow, decreasing the afterload and augmenting diastolic aortic pressure and enhancing diastolic blood flow. This results in better perfusion of the peripheral organs [13]. IABP therapy reduces systolic aortic pressure, which also results in decreased left ventricular wall stress, reducing the myocardial oxygen demand. The inflation and deflation can be triggered by using ECG or the arterial waveform.

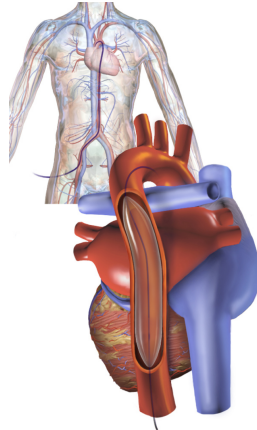


Figure 2.3: Intra-aortic balloon inserted in the aorta via the femoral artery. Image from Wikimedia Commons [10]

Figure 2.3 shows the intra-aortic balloon inserted in the aorta. Intra-aortic balloon pump therapy can be considered in several cases. Some indications for IABP insertion include myocardial infarction and congestive heart failure.

2.2.3 Pneumatic system overview

The intra-aortic balloon pump consists of three main subsystems: the shuttle gas side, the fill manifold and the drive side. The fill manifold is not implemented in this model.

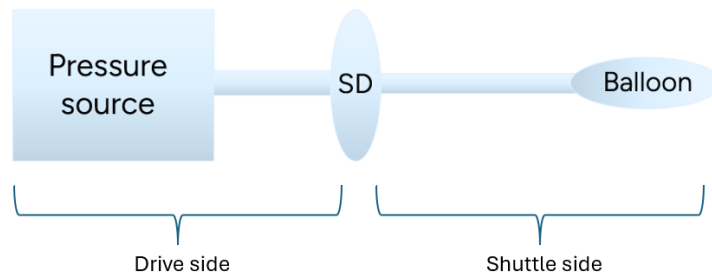


Figure 2.4: Simplified pneumatic scheme of the intra-aortic balloon pump, with the pressure source (drive side), safety disk (SD), tubing and balloon.

The shuttle side includes the intra-aortic balloon catheter, connecting tubing, and the intra-aortic balloon. This part of the system is responsible for the gas exchange between the machine and the balloon. The gas used in the balloon is helium, which is chosen for its low density, allowing rapid inflation and deflation. Helium is added to the shuttle side by the fill manifold.

The drive side of the IABP is responsible for generating and regulating pressures required for inflation and deflation, governed by control logic. This part contains a vacuum reservoir, a pressure reservoir and a compressor that regulates the

pressures in the reservoirs. The drive side also consists of several valves, which opens and closes depending on the inflation and deflation cycle.

Between the drive and shuttle sides, there is a component called the Safety Disk (SD). This consists of a casing with a movable membrane inside that moves in response to pressure changes. During balloon inflation, a valve to the pressure reservoir is opened, creating an overpressure in the drive side and therefore pushing the SD towards the shuttle side, displacing helium to the balloon. During deflation, vacuum is applied when a valve opens to the vacuum reservoir, causing the membrane to move in the opposite direction and draw helium back from the balloon.

Figure 2.4 depicts a simplified pneumatic scheme of the IABP, with a pressure source and the balloon separated by the SD. Connected to the shuttle side is also the fill manifold, not included in the image or this project.

2.3 Literature review

2.3.1 IABP modeling techniques

There have been several studies modeling the intra-aortic balloon pump and its effects on the aortic pressure. Abdolrazaghi, Navidbakhsh, and Hassani [2], studied the effects of intra-aortic balloon pump therapy by creating a mathematical model of the entire cardiovascular system using MATLAB. They constructed a 43-compartment model which simulated physiological conditions accurately, with each compartment being modeled using resistors and capacitors. They simulated myocardial infarction by reducing the left ventricular contractility and the IABP was inserted into the model at the thoracic aorta and was simulated using a Windkessel-type model [27]. They found that after simulating MI, the left ventricular pressure dropped, but with the IABP inserted it returned to closer to normal values. The balloon also helped increase coronary perfusion and reduced left ventricular work.

In 1988, Niederer and Schilt [17] conducted a study using both a simple physical model and a one-dimensional mathematical model. They found that rapid inflation and deflation caused pronounced pressure shocks. By slowing the balloon inflation and deflation, these effects were reduced, but this instead increased sensitivity to the timing of the balloon.

Similarly to Abdolrazaghi, Navidbakhsh, and Hassani [2], De Lazzari et al. [6] created a 0-dimensional electrical circuit representing the cardiovascular system, using resistors, capacitors and inductors to represent vascular resistance, compliance and inertance. The IABP itself was modeled by adding a parallel compliance and resistance to mimic the effects of IABP therapy. This model effectively captured known IABP effects on stroke volume, such as aortic pressure and coronary blood flow. Thin Pa Pa Aye and Naiyanetr [26] also conducted a study of IABP therapy using a lumped parameter model of the cardiovascular system with an electrical analog approach and simulating the main components of the cardiovascular system. The IABP was simulated by introducing pressure,

volume, compliance and resistance into the arterial section of the model. Their results showed that IABP therapy increased mean arterial pressure, reduced cardiac workload and enhanced circulatory support.

Many of the mathematical models of the IABP are made in the electrical domain, since the heart can be represented as an electric circuit, with current and voltage representing flow and pressure, and resistance depending on the fluid and restriction. These studies, however, focus more on being able to model the effects of the IABP therapy, rather than modeling the IABP device itself. This has proven to be an efficient way to model IABP therapy consequences. However, it does not say anything about the machine behind the balloon.

2.3.2 Previous work

This thesis builds upon the foundational work by Zewde Hägglund [32], who developed and validated a dynamic model to simulate the transient gas behavior within the intra-aortic balloon pump. This was made by implementing a model using nonlinear springs and dampers to model the SD and balloon, which effectively captured the system's properties without having to use complex viscoelastic models. Tests were conducted to find the characteristics of the balloon and SD, and tabulated values for the stiffness of the components were used. For the pressure source, a simplified pressure generation was modeled, with two pressure sources that alternated an over and under pressure.

The balloon and SD were modeled using a piston and a spring-damper system. Between these, the tubing was modeled to simulate the shuttle gas side. More details on how this was modeled are covered in Section 3.4.

Experimental validation demonstrated agreement between the model and experimental results. However, the pressure source was simplified and did not maintain pressure over time. The dynamics of the system were not captured over various conditions, indicating that model parameters needed more investigation.

3 Mathematical model

The intra-aortic balloon pump (IABP) is modeled at system level using a lumped-parameter formulation implemented in Simscape (software details in Section 4.1). In a lumped model, each component is treated as a single control volume with spatially uniform states, dynamics come from time variations and block interconnections. This approach neglects spatial gradients within the components and instead focuses on capturing device-level behavior at lower computational cost, since the goal is to understand overall IABP dynamics rather than resolve detailed flow within individual elements.

The IABP model is divided into three subsystems: the drive/pressure source side, the safety disk (SD), and the balloon side. These are connected by medical tubing that transports gas between the SD and the balloon. Since the SD was already implemented in the earlier model with only minor adjustments in this work, the focus here is on the drive side and balloon subsystems. This section first introduces the underlying modeling assumptions and then describes the governing relations and component models for the subsystems.

3.1 Preliminaries

3.1.1 Ideal gas law

In this project, gas behavior is approximated using the ideal gas law. The model assumes that gas molecules are point particles with no volume and no intermolecular forces, interacting only through elastic collisions [29]. Under near-atmospheric pressures and room temperatures, helium and air behave close to ideal, making this assumption reasonable for the operating conditions of the IABP.

The ideal gas relation is written as

$$pV = nR_I T, \quad (1)$$

where P is pressure, V is volume, n is the number of moles, R_I is the universal gas constant, and T is the temperature. Expressed in terms of density, this becomes

$$p = \rho R_{specific} T, \quad (2)$$

where $R_{specific}$ is the specific gas constant.

3.1.2 Compliance and stiffness

In mechanical systems, compliance and stiffness are inverse properties that describe how a material responds to applied force. For a mass-spring system, Hooke's law gives:

$$F = kx \quad (3)$$

where F is the applied force, x the displacement and k the stiffness. A higher stiffness means more force is needed to produce the same displacement. Compliance on the other hand, represents how easy it is to deform a material

under load, and is inverse to the stiffness:

$$C = \frac{1}{k} \quad (4)$$

A system with high stiffness resists deformation and has low compliance, while a system with low stiffness is more flexible and therefore has high compliance. Compliance can also be expressed as

$$C = \frac{\Delta V}{\Delta p}, \quad (5)$$

where ΔV is the change in volume and Δp the change in pressure.

3.1.3 Pressure loss

As gas flows through tubing, friction with the walls causes a pressure drop along the length of the tubing. For laminar, incompressible flow, this can be described by Poiseuille's equation [28]:

$$\Delta p = \frac{8\mu L Q}{\pi r^4}, \quad (6)$$

where μ is the dynamic viscosity, L the pipe length, Q the volumetric flow rate, and r the pipe radius.

In compressible flows, as in this project, the volumetric flow rate varies along the pipe, and the pressure drop must be calculated differently. Equation (6) can still be applied locally if the flow is assumed incompressible over a short section.

More generally, pressure loss can be expressed in terms of a hydraulic resistance:

$$R_{fluid} = \frac{\Delta p}{Q}, \quad (7)$$

where R_{fluid} relates pressure difference across a component to the volumetric flow rate, Q .

3.2 Drive side

The drive side consists of a pressure reservoir, a vacuum reservoir, a scroll compressor, and a set of valves that connect the drive side to the shuttle side via the safety disk. In the real IABP, the compressor speed is regulated by a closed-loop control system to maintain target reservoir pressures. In this model, this control system is not implemented, instead the compressor speed is determined as a function of heart rate using tabulated values identified from experiments, see Section 4.5.1.

In Simscape, the compressor is represented by a **Positive Displacement Compressor (G)** block, where (G) denotes the gas library in Simscape. The block takes angular velocity, ω (rad/s), as input and computes the mass flow rate as

$$\dot{m} = \eta_v \omega \frac{V_{disp}}{V_s}, \quad (8)$$

where η_v is volumetric efficiency, V_{disp} the displacement volume and V_s the specific volume at the inlet, which is calculated from nominal inlet conditions. The displacement is calculated from nominal values $\dot{m}_n, \omega_n, \eta_{v,n}, V_{s,n}$ through the equation

$$V_{disp} = \frac{\dot{m}_n \cdot V_{s,n}}{\omega_n \cdot \eta_{v,n}}. \quad (9)$$

The Simscape schematics of the drive side can be seen in Figure 3.1.

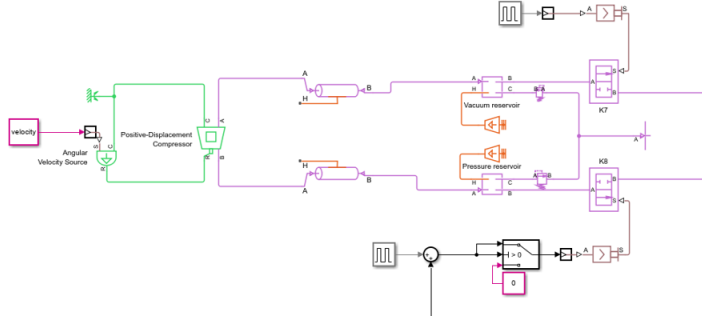


Figure 3.1: Schematics for the drive side of the model. A compressor regulates pressure between two reservoirs and valving with control logic leading to the safety disk.

Speed schedule. The compressor speed is set based on heart rate via a lookup table obtained from experiments (see Section 4.5.1):

Heart rate (bpm)	Compressor RPM
60	1000
80	1200
100	1400

Table 3.1: Compressor RPM values corresponding to different heart rates.

The values in Table 3.1 form the compressor speed schedule used throughout the simulations. Linear interpolation is applied between measured points, while extrapolation is used outside the tabulated range.

3.3 Tubing gas dynamics

Gas transport between the safety disk and the balloon is represented with pipe components, where each pipe component is treated as a single control volume consistent with the lumped formulation introduced earlier. Within each control volume, state variables are assumed spatially uniform and evolve in time according to conservation laws. This resembles a finite-volume discretization, where the properties of a control volume can only change through fluxes across its boundaries.

In Simscape, this is implemented with the **Pipe (G)** block, which models a rigid conduit of a fixed volume filled with compressible gas. The block accounts for the thermal capacitance of the gas and computes transient pressure and temperature dynamics from the conservation of mass, momentum, and energy. This makes the model capable of capturing transient behavior during inflation and deflation.

In the present model, four pipe components are connected in series between the safety disk and the balloon: one to account for dead volume near the safety disk, two representing the extension tubing, and one representing the catheter leading to the balloon. This subdivision reflects the actual tubing geometry and allows resistance effects to be distributed realistically.

Each pipe segment is therefore associated with mass and energy balances, expressed as ODEs, while momentum is included as an algebraic constraint. The corresponding equations are outlined in the following subsections.

3.3.1 Conservation of mass

The mass balance governs how the gas density inside each pipe volume changes with inflow and outflow. The continuity equation expresses conservation of mass:

$$\rho_t + \nabla \cdot (\rho u) = 0, \quad (10)$$

where ρ is the density of the fluid and u the velocity. Integrating over a control volume, CV , yields:

$$\int_{CV} \rho_t dV + \int_{CV} \nabla \cdot (\rho u) dV = 0. \quad (11)$$

Using Gauss's divergence theorem, we get:

$$\int_{CV} \rho_t dV - \int_{CS} \rho u \cdot n dA = 0, \quad (12)$$

where CS is the control volume surface, n the outward normal and A the area of the inlet and outlet of the control volume flow. Define the cell averaged density, with V constant for the rigid pipe, at the internal node I as

$$\rho_I = \frac{1}{V} \int_{CV} \rho dV. \quad (13)$$

The surface integral can be expressed as

$$\int_{CS} \rho u \cdot n dA = \sum_{in} (\rho u A) - \sum_{out} (\rho u A) = \{\text{one inlet, one outlet}\} = (\rho u A)_{in} - (\rho u A)_{out} \quad (14)$$

where the subscripts *in* and *out* denote the inflow and outflow sides of the control volume. This now yields:

$$\frac{d}{dt} \rho_I = \frac{1}{V} ((\rho u A)_{in} - (\rho u A)_{out}) = \frac{1}{V} (\dot{m}_{in} - \dot{m}_{out}) \quad (15)$$

with $\dot{m} = \rho u A$ being the mass flow rate over the boundaries of the control volume. Assuming density is a function of pressure and temperature, $\rho = \rho(p, T)$, the chain rule is used to better understand the pressure and temperature relationship:

$$\frac{d}{dt}\rho_I = \frac{\partial \rho_I}{\partial p} \cdot \frac{dp_I}{dt} + \frac{\partial \rho_I}{\partial T} \cdot \frac{dT_I}{dt} \quad (16)$$

where T_I and p_I are the temperature and pressure at the internal node. To get expressions for the partial derivatives, we look at the ideal gas law:

$$p = \rho R_{specific} T \Rightarrow \rho = \frac{p}{R_{specific} T} \quad (17)$$

and get, with the subscript I marking the value at the internal node:

$$\frac{\partial \rho_I}{\partial p} = \frac{1}{R_{specific} T_I} = \frac{\rho_I}{p_I} \quad (18)$$

and

$$\frac{\partial \rho_I}{\partial T} = -\frac{p_I}{R_{specific} T_I^2} = -\frac{\rho_I}{T_I} \quad (19)$$

We can now rewrite our equation as:

$$\frac{\rho_I}{p_I} \cdot \frac{dp_I}{dt} - \frac{\rho_I}{T_I} \cdot \frac{dT_I}{dt} = \frac{1}{V} (\dot{m}_{in} - \dot{m}_{out}). \quad (20)$$

Equation (20) corresponds to one ODE governing pressure and temperature within each pipe block in Simscape. This, together with the energy balance below, forms the dynamic ODEs for each pipe control volume. The mass flow rates over the boundaries are calculated using the upwind scheme, using the temperature and pressure from the upwind cell or block.

3.3.2 Conservation of momentum

The conservation of momentum is included as an algebraic constraint in the gas pipe model. For each pipe element, the momentum balance over a control volume can be written as

$$\int_{CV} (\rho u)_t dV + \int_{CS} (\rho u^2 n) dA = \sum F. \quad (21)$$

Where ρ is the density of the gas, u the velocity and $\sum F$ the sum of forces acting on the control volume. Neglecting the time derivative of momentum, and rewriting the surface integral gives:

$$\int_{CS} (\rho u^2 n) dA = (\rho u A)_{in} - (\rho u A)_{out} = (\dot{m} u)_{in} - (\dot{m} u)_{out} \quad (22)$$

with $\dot{m} = \rho u A$ denoting the mass flow rate through a port of cross-sectional area A .

Dividing the control volume into two halves, we denote the inlet by subscript in and the internal node by I . Since mass flow is conserved, $\dot{m}_{in} = \dot{m}_I$, and

the velocities can be written as $u_{in} = \dot{m}_{in}/(\rho_{in}A)$ and $u_I = \dot{m}_{in}/(\rho_I A)$. The momentum flux difference then becomes

$$(\dot{m}u)_{in} - (\dot{m}u)_{out} = \dot{m}_{in} \frac{\dot{m}_{in}}{\rho_{in}A} - \dot{m}_{in} \frac{\dot{m}_{in}}{\rho_I A}. \quad (23)$$

The net force acting on the half control volume is

$$\sum F = Ap_{in} - Ap_I - A\Delta p_{in,I}. \quad (24)$$

Here, p_{in} denotes the gas pressure at the inlet port, and p_I the pressure at the internal node between the two half control volumes. $\Delta p_{in,I}$ represents the pressure loss due to viscous friction. Combining this with (23) yields

$$\begin{aligned} A(p_{in} - p_I - \Delta p_{in,I}) &= \frac{\dot{m}_{in}^2}{A} \left(\frac{1}{\rho_{in}} - \frac{1}{\rho_I} \right) \\ \Rightarrow p_{in} - p_I &= \left(\frac{\dot{m}_{in}}{A} \right)^2 \left(\frac{1}{\rho_{in}} - \frac{1}{\rho_I} \right) + \Delta p_{in,I}. \end{aligned} \quad (25)$$

An analogous expression is obtained for the outlet side. These relations define algebraic constraints that are solved together with the conservation of mass and energy.

Viscous friction losses. The viscous friction term Δp is modeled with the Darcy-Weisbach equation:

$$\Delta p = f \cdot \frac{L_{total}}{D} \cdot \frac{\rho u^2}{2} \quad (26)$$

where f is the Darcy friction factor, L_{total} is the effective pipe length, and D the hydraulic diameter. The friction factor depends on the flow regime, which is determined by the Reynolds number

$$Re = \frac{2ru\rho}{\mu}, \quad (27)$$

where r is the radius of the pipe. For $Re < 2000$ the flow is considered laminar, while for $Re > 4000$ it is turbulent, with different correlations for f applied in each case.

3.3.3 Conservation of energy

Similarly, for the conservation of energy over a control volume using a finite volume method, we use the first law of thermodynamics for a fixed control volume. For an ideal gas, the internal energy U is given by

$$U = nc_v T_I = \frac{p_I \cdot c_v \cdot V}{R} \quad (28)$$

where n is the number of moles, c_v the heat capacity at constant volume, T_I temperature, R the universal gas constant, V the volume and p_I the internal

pressure. The cell-averaged internal energy is defined as:

$$U_I = \frac{1}{V} \int_{CV} U dV. \quad (29)$$

Applying the first law of thermodynamics to the control volume yields

$$\frac{dU_I}{dt} = \frac{1}{V}(\Phi_{in} - \Phi_{out}) + Q_H, \quad (30)$$

where Φ_{in} and Φ_{out} denote the energy fluxes through the inlet and outlet, and Q_H is the heat flow rate. To express the internal energy change in terms of temperature and pressure, we use the thermodynamic identity

$$\frac{dU_I}{dt} = V(\beta_T p_I - \alpha T_I) \frac{dp_I}{dt} + (c_p - \alpha p_I V) \frac{dT_I}{dt} \quad (31)$$

where α is the coefficient of thermal expansion, β_T the isothermal compressibility and c_p the heat capacity at constant pressure. Combining the finite-volume balance with this thermodynamic relation we get a conservation of energy equation analogous to the mass and momentum equations in Sections 3.3.1 and 3.3.2. The full expression is not reproduced here since Simscape uses a rearranged form of this relation, but the governing structure follows from the equations above.

3.3.4 Pipe fittings and bending

The Equivalent Length method is a simplified approach used in fluid mechanics and piping system design to account for pressure losses caused by fittings, valves, bends and other components in addition to the losses from straight pipes. Each fitting introduces resistance to fluid flow, and produces a pressure drop that is comparable to that of a certain length of straight pipe. The method uses this approach by assigning an equivalent length to each component, which represents the length of straight pipe that would cause the same pressure loss.

When calculating friction losses, the total effective length of the system is then calculated as

$$L_{total} = L_{pipe} + L_{equiv} \quad (32)$$

where L_{pipe} is the actual length of the pipe and L_{equiv} is the equivalent length for a fitting, bend or valve. Once the equivalent length is obtained, equations such as the Darcy-Weisbach equation can be applied as if the system consisted of only straight pipe. For common fittings, tabulated equivalent length data is available.

In the previous model, the equivalent length of fittings was mistakenly set equal to the actual length of the tubing. This significantly overestimated the resistance. In this project, this was corrected by removing the equivalent length contribution entirely. While this may underestimate minor local losses from connectors, it is probable that the dominant losses in narrow medical tubing arise from viscous friction in the straight sections. This simplification was therefore deemed reasonable.

3.4 Balloon subsystem

The balloon subsystem follows the Simscape implementation developed by Zewde Hägglund [32]. In this work, two changes were introduced: (i) replacing the nonlinear spring-damper with a calibrated linear spring-damper, and (ii) adding check valves to reproduce observed inflation/deflation threshold behavior. With changes made to the rest of the model, the nonlinear spring-damper approach was also examined further.

In Simscape, the balloon is modeled as a gas volume connected to a mechanical spring-damper system via a **Translational Mechanical Converter** (TMC). The TMC represents an interface between a pneumatic system and a mechanical one. Its volume varies with mechanical displacement, given by:

$$V = V_{dead} + S \cdot x_b \cdot \varepsilon, \quad (33)$$

where V_{dead} is the dead volume of the TMC, S the cross-sectional area and $\varepsilon \in \{+1, -1\}$ is the mechanical orientation coefficient. A hard stop is enforced on x_b when the balloon maximum volume is reached, implemented using a **Translational Hard Stop**.

Let ρ_I , T_I , p_I , h_I denote the density, temperature, pressure and specific enthalpy of the gas in the TMC control volume. With mass inflow \dot{m}_{in} and energy flow Φ_{in} defined positive into the control volume, the balance equations for the deforming, rigid wall TMC are:

$$\frac{d}{dt}(\rho_I V) = \dot{m}_{in} \quad (34)$$

for mass, and expressing it in p_I, T_I using $\rho_I = \rho_I(p_I, T_I)$, gives

$$V \left(\frac{\rho_I}{p_I} \cdot \frac{dp_I}{dt} - \frac{\rho_I}{T_I} \cdot \frac{dT_I}{dt} \right) + \rho_I \frac{dV}{dt} = \dot{m}_{in}. \quad (35)$$

The conservation of energy is similar to that of the **Pipe (G)** block, with an additional term accounting for the change in gas volume and the pressure-volume work. The conservation of energy is given by:

$$V \left(\frac{h_I}{ZRT_I} - 1 \right) \cdot \frac{dp_I}{dt} + V\rho \left(c_p - \frac{h_I}{T_I} \right) \frac{dT_I}{dt} + \rho_I h_I \frac{dV}{dt} = \Phi_{in} + Q_H. \quad (36)$$

On the other side of the spring-damper, a second TMC is mounted with opposite orientation. When the spring extends, this TMC's volume decreases, and it displaces gas into an external volume that represents a compliance chamber, imposing a back-pressure on the balloon side. Figure 3.2 shows the schematics of the balloon.

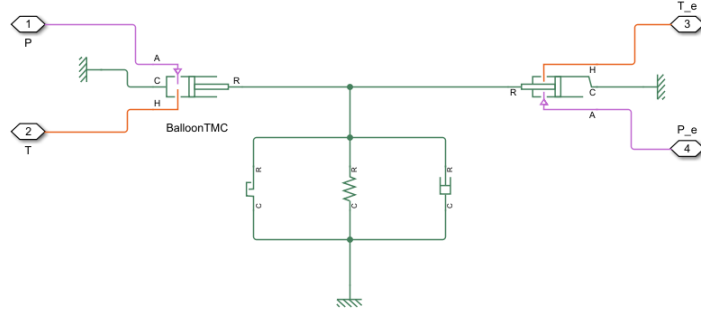


Figure 3.2: Balloon subsystem with opposing TMCs and spring-damper (adapted from [32]). The translational mechanical converter (TMC) to the left accounts for the balloon volume. The spring-damper system is pushed when pressure is applied to the TMC, pushing the opposite TMC in the other direction. Pressure is applied to the right TMC, simulating a back pressure from a compliance chamber.

As mentioned, a nonlinear spring and damper was used in the previous model, and the stiffness of the nonlinear spring was calculated from experiments.

3.4.1 Spring-damper system

The mechanical load on the gas volume is represented by a spring-damper connected to the TMC. The force is modeled as

$$F_m = m\ddot{x}_b + c\dot{x}_b + kx_b. \quad (37)$$

where x_b is the TMC displacement, m the mass, c the damping coefficient and k the stiffness. If static, this reduces to Hooke's law (3).

To capture nonlinear elasticity, the force can be specified either by an explicit law:

$$F(x) = \sum_{n=1}^N a_n x^n \quad (38)$$

or by tabulated data $F(x)$ derived from pressure volume measurements. The previous model used the tabulated option. In this work, a linear spring is instead tested, along with using check valves.

3.4.2 Valve threshold model for balloon dynamics

It is well established that the pressure-volume relationship of a balloon does not follow Hooke's law due to the nonlinear elastic properties of its material, and often exhibits a threshold behavior: once a cracking pressure is reached, inflation becomes easier [15]. To reproduce this effect without a nonlinear spring law, this work introduces check valves that remain closed until a prescribed pressure differential is reached, mimicking the observed delay in inflation and deflation.

Two blocks of **Check Valve (G)** are placed in the shuttle path with opposite orientations, one governing inflation and one governing deflation, as can be seen in Figure 3.3.

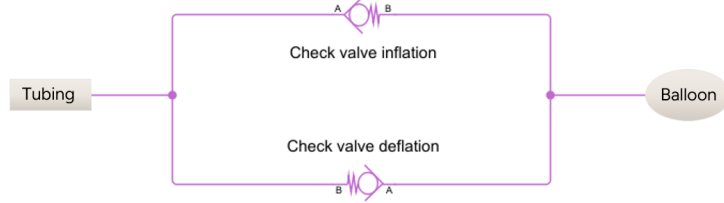


Figure 3.3: Model setup for the check valve approach in Simscape, with one check valve representing inflation cracking pressure behavior and one for deflation.

For a valve oriented from port A to B , the control pressure is defined as

$$P_{Ctl} = P_A - P_B, \quad (39)$$

The valve begins to open when $P_{Ctl} > P_{Crk}$, where P_{Crk} is a predefined pressure threshold, and is fully open when the pressure reaches P_{Max} . A normalized control pressure is used:

$$\hat{P} = \frac{P_{Ctl} - P_{Crk}}{P_{Max} - P_{Crk}} \quad (40)$$

and the opening fraction is determined by

$$L = (1 - L_{leak})\hat{P} + L_{leak}, \quad (41)$$

where the leakage is set to $L_{leak} \approx 10^{-16}$. The two TMCs are connected by a softer intermediate spring-damper to retain the mechanical interface while the valves control the gas flow, which captures the threshold behavior mentioned earlier.

3.5 Model adjustments for resistance behavior

In Simscape, gas properties for each component of the pneumatic system are defined using a **Gas Properties** block. The default settings for this block is dry air, but the shuttle-side part of the system operates with helium and therefore needs an accurate representation of its properties. Upon review, it was found that the previously defined gas properties did not accurately reflect those of helium. After correcting the gas definition, the model behavior changed notably, and the model had to be adjusted.

Despite the property corrections, along with dimension changes in the model, a mismatch remained between simulations and measurements. This was seen as a missing flow resistance in the shuttle side. The tubing and balloon geometry matched specifications, and equivalent length contributions for fittings were

removed, as mentioned in Section 3.3.4, to avoid overestimation. To account for losses that were not captured by friction losses alone, a **Local Restriction (G)** block was introduced as a gathered loss element.

The restriction was positioned between the tubing and balloon, representing minor pressure losses with a single element. After calibration, the model reproduced the observed pressure trajectories while preserving the physically reasonable tubing parameters established earlier.

4 Method

4.1 Software

The model in this project is implemented using Simscape, an extension of the MATLAB-based graphical programming environment Simulink [25]. Simulink provides a programming interface based on block diagrams, with an extensive and customizable library of components for modeling, simulation and control design.

Simscape is specifically designed for modeling physical systems across multiple domains, such as mechanical, electrical, fluid and gas, within the Simulink framework. It allows users to represent physical components using predefined blocks, or to create custom components using the MATLAB-based Simscape language. Simscape is integrated with MATLAB scripting, allowing parameter specification, automation and post-processing.

Additionally, Simscape allows C code generation, making it possible to deploy models to other simulation platforms, which can be useful for integration into larger software pipelines.

4.2 Differential-algebraic equations

The equations governing the Simscape model take the form of differential-algebraic equations (DAEs). In general, a system can be written in implicit form as

$$F(t, x, x') = 0, \quad (42)$$

where x and x' may be vectors. If the Jacobian $\frac{\partial F}{\partial x'}$ is non-singular, the system reduces to an ordinary differential equation (ODE). When this Jacobian is singular, some equations contain no derivatives, making them algebraic constraints and therefore a DAE system.

A simple and well-studied case is the linear constant-coefficient DAE

$$Ax'(t) + Bx(t) = f(t), \quad (43)$$

which is the best understood class of DAE systems and have been studied for many years, particularly in control theory and electrical engineering [4]. More generally, DAEs may be time-varying or nonlinear, where analytical treatment is considerably more difficult.

Index. A key concept in DAE analysis is the differentiation index, which measures how many times the algebraic equations must be differentiated to obtain an explicit ODE system. Most numerical methods require index-1 systems, where the derivatives can be determined directly from the equations. Higher-index systems typically need to be reformulated or reduced before simulation.

Equation assembly in Simscape. The created block network is compiled by Simscape into a single DAE system

$$M(x) x' = f(x, z, t), \quad 0 = g(x, z, t). \quad (44)$$

Here x collects the differential states across domains, e.g.

$$x = [p_1, T_1, \dots, p_N, T_N, x_b, v_b]^T, \quad (45)$$

with (p_i, T_i) being the gas states in volumes and (x_b, v_b) the balloon-side mechanical displacement and velocity, and M contains, among other things, the mass/energy coefficients from the conservation laws in Section 3 and g enforces algebraic constraints. Simscape then constructs the equations into an index-1 formulation and computes initial conditions and then solves the system with the selected solver, discussed in Section 4.4.1.

4.3 Backward and numerical differentiation formulas

Backward differentiation formulas. For solving stiff differential equations, a common approach is to use Backward Differentiation Formulas (BDFs). These are implicit multistep formulas particularly suited for stiff problems due to their stability properties. A general BDF of order p can be written as:

$$y_{n+1} + \sum_{s=0}^{p-1} \alpha_{n-s} y_{n-s} = h\beta f(t_{n+1}, y_{n+1}), \quad (46)$$

where h is the time step from time t_n to t_{n+1} , α_{n-s} and β are method-dependent coefficients chosen to achieve order p , and f is the derivative function. This is an algebraic equation that is solved with Newton-Raphson iteration. For MATLAB's solvers, the iteration is started with a predicted value:

$$y_{n+1}^{(0)} = \sum_{m=0}^p \nabla^m y_n. \quad (47)$$

For most solvers using BDFs, a quasi-constant time step size is used. This means that the time step is constant, unless some event requires it to change to maintain stability. These methods also often vary between orders when integrating. The most trivial example of a BDF is the implicit Euler method:

$$y_{n+1} = y_n + hf(t_{n+1}, y_{n+1}). \quad (48)$$

Numerical differentiation formulas. To improve upon standard BDFs, Numerical Differentiation Formulas (NDFs) were introduced [14]. These methods incorporate the predictor, (47), into the equation to improve stability and efficiency. An NDF of order p can be written as:

$$y_{n+1} + \sum_{s=0}^{p-1} \alpha_{n-s} y_{n-s} - h\beta f(t_{n+1}, y_{n+1}) - \kappa\gamma_p (y_{n+1} - y_{n+1}^{(0)}) = 0, \quad (49)$$

where

$$\gamma_p = \sum_{j=1}^p \frac{1}{j}. \quad (50)$$

and κ is a scalar parameter. The algebraic equation for y_{n+1} can be solved using a simplified Newton chord iteration [22].

The numerical differentiation formula of order 2 is given by

$$y_{n+1} - \frac{3}{2}y_n + \frac{3}{5}y_{n-1} - \frac{1}{10}y_{n-2} = \frac{3}{5}hf(t_{n+1}, y_{n+1}) \quad (51)$$

which the solver `daessc` is based on. The numerical differentiation formula of order 2 has the same order of accuracy as BDF of order 2, but for sufficiently small step sizes it can achieve the same accuracy with larger time steps [22].

4.4 Simulation framework

MATLAB provides several different solvers for ordinary differential equations (ODEs), capable of both handling explicit ODEs of the form:

$$y' = f(t, y), \quad (52)$$

and linearly implicit ODEs of the form

$$M(t, y)y' = f(t, y), \quad (53)$$

where $M(t, y)$ is a non-singular mass matrix. MATLAB solvers also support fully implicit ODEs of the form $f(t, y, y') = 0$. The choice of solver depends on the characteristics of the problem, such as stiffness, accuracy requirements and problem size.

For non-stiff systems, the standard solver in MATLAB is the `ode45` solver, which implements a Dormand-Prince (4,5) Runge-Kutta method with adaptive time-stepping. This method is usually the default choice for the Simulink model explorer solver [8] and offers a good balance between performance and accuracy for non-stiff systems.

A problem is considered stiff when it contains dynamics evolving at different time scales, making explicit methods inefficient or unstable. This is common in physical systems with components that change rapidly relative to the rest of the system, such as rapid valve openings. For stiff or moderately stiff problems, MATLAB offers several different solvers:

- `ode23` is a lower order solver based on the Bogacki-Shampine (2,3) pair [3] and can be more efficient than `ode45` for problems requiring lower accuracy or for moderately stiff systems.
- `ode15s` is a variable-step, variable order solver based on the numerical differentiation formulas and backward differentiation formulas, MATLAB's `ode15s` solver uses NDFs of order 1 to 5 [22], and can also use standard BDFs

when necessary, although NDFs are typically more efficient. This solver can be used for stiff systems and when solving differential-algebraic equations.

- `ode23s` is designed for stiff systems and requires a constant mass matrix. It is based on the Rosenbrock formula of order 2 and is a single-step solver, making it potentially more efficient than `ode15s` when solving problems allowing lower accuracy or if there are problems with solutions that vary rapidly.
- `ode23t` can handle differential-algebraic equations of index 1, and utilizes the trapezoidal rule. For a problem that is moderately stiff, this solver can be preferable over `ode15s`, and when a solution without numerical damping is needed.
- `daessc` is a Simscape-exclusive solver designed for index-1 differential-algebraic equations with strong algebraic components. It is based on a second-order numerical differentiation formula. The use of `daessc` in this project is discussed further in Section 4.4.1.

In summary, while multiple stiff and DAE-capable solvers exist, the Simscape model generates index-1 DAEs due to algebraic constraints from component connections and the numerical method below are chosen with this structure in mind.

4.4.1 Solver choice

For the simulations in this project, the solver `daessc` was selected. This solver is specifically designed for stiff systems of differential-algebraic equations (DAEs) with strong algebraic constraints, which are characteristic of the physical models generated in Simscape. Furthermore, `daessc` is recommended by MathWorks for Simscape models, as it is tuned for problems dominated by algebraic parts. For these reasons, `daessc` was chosen as the default solver for this project.

4.5 Experimental work

To parameterize and validate the model, two sets of experiments were performed. First, compressor characterization tests were conducted to estimate parameters of the positive-displacement compressor model and assess its isolated behavior. Second, balloon inflation tests were carried out under controlled external pressures to calibrate the balloon dynamics and validate the overall model response. The setup and procedure for each experiment are described in the following subsections.

4.5.1 Compressor characterization

For the tests on the compressor, both the vacuum and pressure reservoirs were first vented to atmosphere. After pressures equalized, the vents were closed and the compressor was driven at a constant speed. Two speeds were tested, 800 RPM and 1200 RPM. For each run, the pressure in the vacuum reservoir was recorded from the time the compressor started until the pressure reached its target level.

In addition, a LPM-RPM performance curve from the company was provided and was treated as a secondary target to try to ensure that parameters remained consistent with machine behavior.

Complementary data was collected during active therapy mode to observe how the compressor maintained reservoir pressures under realistic conditions. These data were used for validation.

4.5.2 Balloon inflation and validation tests

To calibrate and validate the balloon dynamics under different environmental pressures, a 40 cc intra-aortic balloon was placed in a compliance chamber with adjustable external pressure. The chamber was then pressurized to three levels: 25 mmHg, 50 mmHg, and 100 mmHg (gauge). At each setting, the IABP was run in therapy mode at three heart rates: 60, 80 and 100 bpm. For each run, the shuttle side pressure, drive side pressures and the chamber/external pressure were logged.

Test #	Compliance chamber pressure (mmHg)	Heart rate (bpm)
1		60
2	25	80
3		100
4		60
5	50	80
6		100
7		60
8	100	80
9		100

Table 4.1: Table showing the different experiments conducted with the IABP, with different external pressures and heart rates.

The data were then used to tune balloon side parameters, and to validate the shuttle pressure dynamics. Tuning followed the least-squares procedure in Section 4.6. For each setting, simulated and measured signals were compared and the tests in Table 4.1 were used to assess robustness of the model.

4.6 Parameter estimation

The model contains many parameters that influence its behavior, and one effective method for determining suitable values is through optimization. The estimation error between the simulated response, y_{sim} and the reference signal, y_{ref} , can be defined as

$$e(t) = y_{ref} - y_{sim} \quad (54)$$

where x is the parameter vector to estimate. The vector of residuals is defined as:

$$F(x) = \begin{bmatrix} e(0) \\ e(1) \\ \vdots \\ e(N) \end{bmatrix}$$

This is then set up as an optimization problem using least squares:

$$\begin{aligned} \min_x & \|F(x)\|_2^2 \\ \text{s.t.} & \hat{x} \leq x \leq \bar{x} \end{aligned} \quad (55)$$

where \hat{x} and \bar{x} denote the lower and upper bounds on the design variables, and $F(x)$ is composed of the residuals at each time step. The problem was solved using MATLAB's `lsqnonlin` function from the Optimization Toolbox [24].

For this project, parameter tuning was performed using MathWorks' Parameter Estimator app, part of the Simulink Design Optimization toolbox. This program simplifies the setup of parameter estimation problems by allowing the user to define model parameters, specify experimental data, and configure bounds and cost functions in a graphical interface.

4.6.1 Case 1: Check-valve parameters

For the check valve balloon approach, the parameters to estimate were the cracking and fully open pressure thresholds:

$$x = \begin{bmatrix} P_{Crk} \\ P_{Max} \end{bmatrix}, \quad (56)$$

The reference and simulated signals were the shuttle-side pressures

$$y_{ref}(t) = P_{shuttle,ref}(t), \quad y_{sim}(t) = P_{shuttle,sim}(t) \quad (57)$$

Parameters were updated iteratively until the simulated pressure matched the measured pressure optimally over each experiment.

4.6.2 Case 2: Compressor variables

For the drive side, the measured signal was the vacuum reservoir pressure. The estimated parameters were nominal values for the compressor's mass flow production:

$$x = \begin{bmatrix} \eta_{v,n} \\ \dot{m}_n \\ \omega_n \end{bmatrix} \quad (58)$$

where $\eta_{v,n}$ is the nominal volumetric efficiency, \dot{m}_n is the nominal mass flow rate and ω_n the nominal shaft speed. For this problem, residuals were built from:

$$y_{ref}(t) = P_{vac,ref}(t), \quad y_{sim}(t) = P_{vac,sim}(t) \quad (59)$$

The fitting was performed on the signals mentioned in Section 4.5.1 to try and identify parameters that reproduce the observed pressure curves. Figure 4.1 displays the signals.

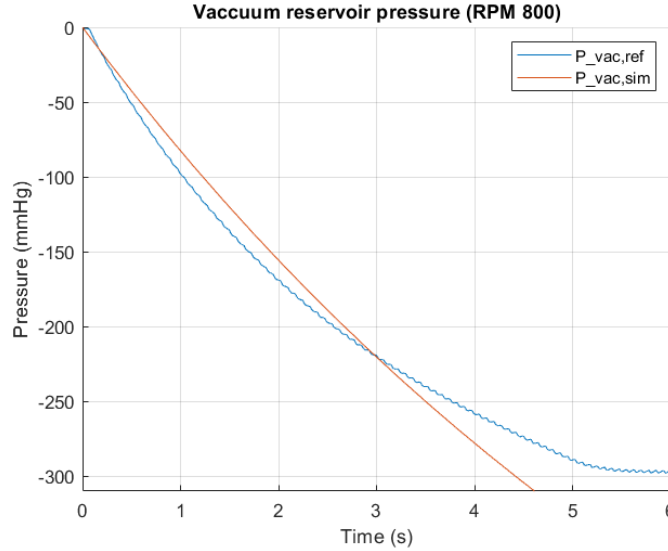


Figure 4.1: The signals used in the parameter estimation for the compressor variables. Blue line represents pressure measured in experiments, while the red line is the pressure calculated in Simscape. The error between the curves is calculated in each iteration and the parameters are updated accordingly.

The blue line in Figure 4.1 displays the measured signal from experiments, while the red line is the model response.

4.7 Use case: Altitude test

This section presents the altitude test as a use case for the model. Here, the tuned model was evaluated under conditions of practical relevance to the company. This was to assess whether the model can reproduce desired device behavior when atmospheric pressure changes with altitude and when heart rate varies. The IABP device should be able to operate over different altitudes, and therefore this is a relevant use case for this model.

When testing the real IABP, the back pressure is altered depending on atmospheric pressure, which was implemented in the model for atmospheric pressures ranging from 450 to 760 mmHg. For each pressure, the heart rate was varied from 30 to 200 bpm. For every combination, the model calculated the balloon's 10-90 % inflation and deflation times, required to be ≤ 0.12 s. The maximum inflation volume was also calculated and is required to remain within specified limits.

At therapy initiation, the IABP device estimates the deflation vacuum level so that the balloon can reach the target full inflation volume. The model can

serve as a way to test different alternative algorithms for this estimation. In the implementation, two algorithms were assessed, and the results most relevant to this study are included in the report, noting that the model can be used to prototype and compare different control strategies.

4.8 Modified equation analysis

To analyze the numerical properties of the NDF2 scheme used in the chosen solver `daessc`, we can derive its modified equation. This shows how the discrete method deviates from the exact ODE, and whether it introduces numerical damping (dissipation) or phase errors (dispersion). For an ODE of the form

$$\frac{d}{dt}\mathbf{r}(t) = \mathbf{f}(\mathbf{r}(t)) \quad (60)$$

the NDF2 discretization is

$$\frac{\mathbf{r}_{n+1} - \frac{3}{2}\mathbf{r}_n + \frac{3}{5}\mathbf{r}_{n-1} - \frac{1}{10}\mathbf{r}_{n-2}}{\frac{3}{5}\Delta t} = \mathbf{f}_{n+1}. \quad (61)$$

To obtain the modified equation, we introduce a test function $\mathbf{v}(t)$ that satisfies (61) exactly. By expanding \mathbf{v} in Taylor series, we can identify the leading perturbation terms added by the method. Expanding \mathbf{v} about t gives

$$\begin{aligned} \mathbf{v}(t + \Delta t) &= \mathbf{v} + \Delta t\mathbf{v}' + \frac{\Delta t^2}{2}\mathbf{v}'' + \frac{\Delta t^3}{3!}\mathbf{v}''' + \frac{\Delta t^4}{4!}\mathbf{v}'''' + O(\Delta t^5) \\ \mathbf{v}(t - \Delta t) &= \mathbf{v} - \Delta t\mathbf{v}' + \frac{\Delta t^2}{2}\mathbf{v}'' - \frac{\Delta t^3}{3!}\mathbf{v}''' + \frac{\Delta t^4}{4!}\mathbf{v}'''' + O(\Delta t^5) \\ \mathbf{v}(t - 2\Delta t) &= \mathbf{v} - 2\Delta t\mathbf{v}' + \frac{4\Delta t^2}{2}\mathbf{v}'' - \frac{8\Delta t^3}{3!}\mathbf{v}''' + \frac{16\Delta t^4}{4!}\mathbf{v}'''' + O(\Delta t^5) \end{aligned} \quad (62)$$

Substituting these expansions into (61) and simplifying yields

$$\mathbf{v}' = \mathbf{f} - \frac{1}{75}\Delta t^2\mathbf{v}''' + O(\Delta t^4).$$

Therefore, the modified equation is

$$\mathbf{v}' = \mathbf{f} - \frac{1}{75}\Delta t^2\mathbf{v}''' \quad (63)$$

The perturbation term involves only odd derivatives, which indicates that the method introduces numerical dispersion rather than dissipation. This means that numerical errors primarily shift the timing of pressure signals, rather than damping their amplitude. In the pneumatic flow, this appears as small phase shifts in the propagation of pressure waves, the peaks may arrive slightly earlier or later than expected, but their magnitude is preserved. Even at small step sizes, these timing errors can remain and may accumulate over long simulations.

5 Results

This section presents the results from different simulations. All pressures are plotted as gauge, where 0 mmHg corresponds to atmospheric pressure. Units are millimeters of mercury (mmHg) if not stated otherwise.

The results are presented to show how each part of the system works under simulation. On the drive side, the drive side pressure and the vacuum reservoir pressure are presented. These plots indicate whether the system can maintain stable pressure levels during operation. On the other side of the safety disk, the focus is placed on the shuttle side pressure.

Three balloon models are compared: (i) nonlinear spring-damper, (ii) linear spring-damper, and (iii) the check valve approach. This is to examine whether the check-valve design improves accuracy relative to the models with only springs.

In addition, the pressure in the compliance chamber is presented to illustrate the inflation and deflation behavior of the balloon. Finally, results from the altitude test use case are presented.

5.1 Drive side

The drive side pressure is the pressure between the reservoirs and the safety disk (SD). It pushes and pulls the SD membrane, triggering balloon inflation and deflation.

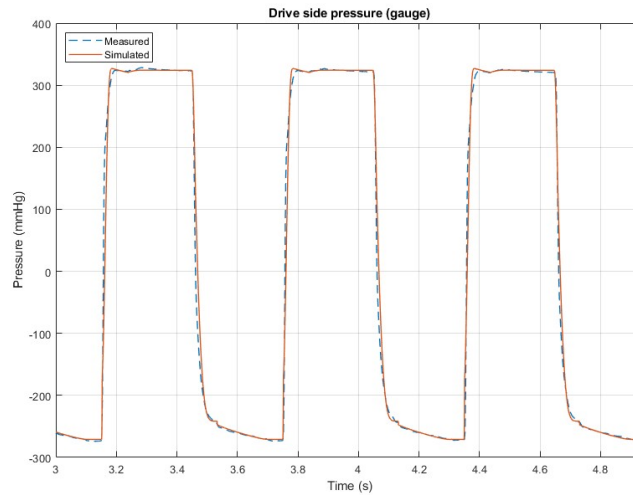


Figure 5.1: Drive side pressure at 100 bpm. Measured pressure is shown in blue and the simulated pressure is red. Pressures are gauge (mmHg).

Figure 5.1 shows the expected valve-driven pressure pattern. At the start of diastole, the pressure valve opens, producing a rapid rise in drive pressure, to

around 320 mmHg. The valve then closes, isolating the drive pressure until deflation. When the vacuum valve opens, around $t \approx 3.45$ s, the drive pressure equalizes with the vacuum reservoir and the pressure drops sharply to around -240 mmHg. While the vacuum valve remains open, the drive pressure adjusts as the reservoir pressure is being lowered by the compressor. After the vacuum valve closes, around $t \approx 3.7$ s, the drive pressure reaches a plateau before the next cycle begins. Overall, the simulation reproduces the timings and amplitudes of the positive and negative plateaus with some discrepancies near valve transitions.

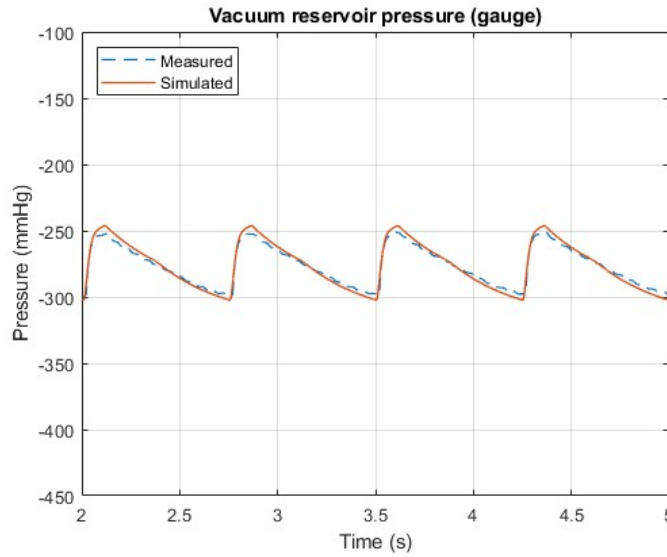


Figure 5.2: Vacuum reservoir pressure at 100 bpm. Measured signal is shown in blue and simulated in red. Pressures are gauge (mmHg).

Figure 5.2 shows the corresponding vacuum reservoir pressure. Each time the vacuum valve opens to deflate the balloon, the reservoir partially equalizes with the drive manifold, producing a step increase. Between openings, the compressor pulls the reservoir back to the target pressure level. The model captures this step and recover behavior, with some minor inconsistencies.

Although the reservoir pressures follow the expected cycle, the compressor subsystem does not reproduce the measured vacuum ramp rates or the LPM–RPM characteristic mentioned in Section 4.5.1, even at atmospheric pressure. In other words, reasonable system-level behavior is achieved even though there is a component-level mismatch.

5.2 Shuttle pressure (balloon subsystem results)

The shuttle side pressure is the driver of balloon inflation and deflation. The balloon model determines how pressure produces volume change, therefore different balloon models result in different pressure-displacement relationships.

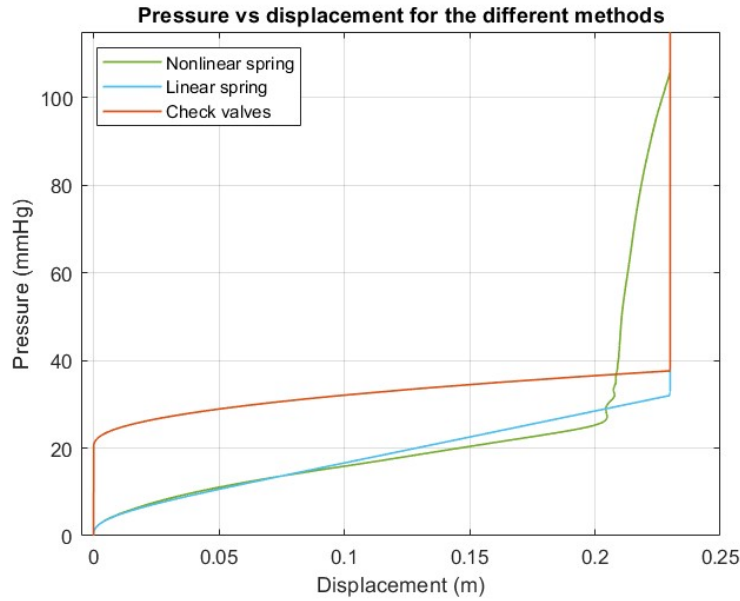


Figure 5.3: Balloon pressure-displacement curves for the three approaches. Green: nonlinear spring-damper, blue: linear spring damper, red: check valve model. The check valve model exhibits a threshold region before displacement occurs.

Figure 5.3 illustrates the pressure-displacement behavior for the different balloon models. The linear model produces a linear pressure-displacement relation until it reaches the hard stop while the nonlinear spring shows increasing stiffness at larger displacements. The check valve model displays a clear threshold, the pressure rises without any displacement until the cracking pressure level is exceeded, after which displacement increases rapidly.

Check valve approach, 50 mmHg chamber pressure, 80 bpm. When running the simulation with heart rate 80 bpm and environmental pressure $P_{env} = 50$ mmHg, we get the following result using the check valve approach:

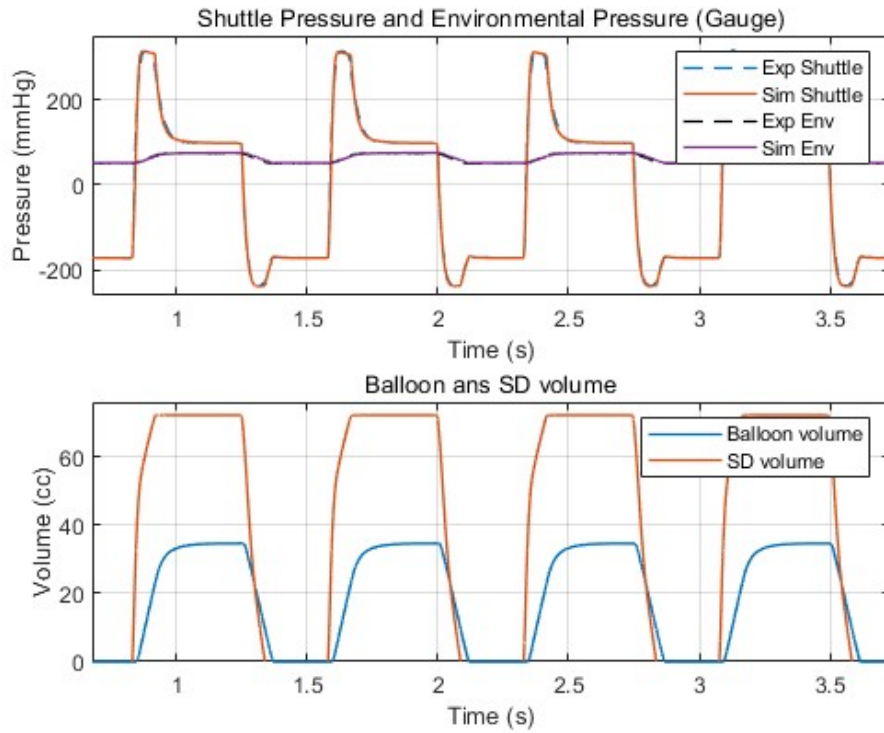


Figure 5.4: Environmental pressure 50 mmHg (gauge), heart rate 80 bpm. Top: shuttle pressure and chamber/environmental pressure. Measured results are shown as dotted while simulated results are solid lines. Shuttle: blue dotted (*Exp Shuttle*), simulated response red solid (*Sim Shuttle*). Chamber: black dotted (*Exp Env*), purple solid (*Sim Env*). Bottom: simulated balloon and SD volumes.

In Figure 5.4, the shuttle pressure rises rapidly to ≈ 320 mmHg at the start of inflation, then settles to a plateau as flow distributes into the tubing and balloon. During deflation, the shuttle pressure drops below -200 mmHg before reaching a deflation plateau. Chamber pressure (shown in purple and black) varies in phase with balloon volume, showing the inflation and deflation timing.

Higher heart rate and lower chamber pressure (25 mmHg, 100 bpm). Looking at another environmental pressure in the compliance chamber, we get the following plot:

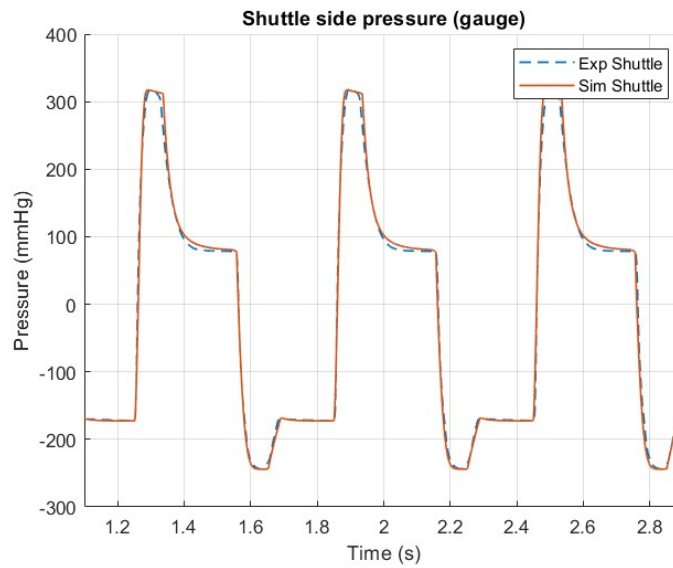


Figure 5.5: Shuttle pressure at 25 mmHg chamber pressure and 100 bpm. Blue dotted line: measured shuttle pressure, red solid line: simulated shuttle pressure.

At higher heart rate and lower chamber pressure, as seen in Figure 5.5, inflation time is shorter and the shuttle pressure does not fully settle to a plateau before deflation begins, yielding a higher peak than in experiments.

5.2.1 Comparison of balloon models

Waveform comparison at 50 mmHg chamber pressure. After alterations done to the rest of the model, the different balloon modeling approaches yield similar results, especially in the best case scenario, which is when the compliance chamber is set to a pressure of 50 mmHg (gauge). This can be seen in the following plot:

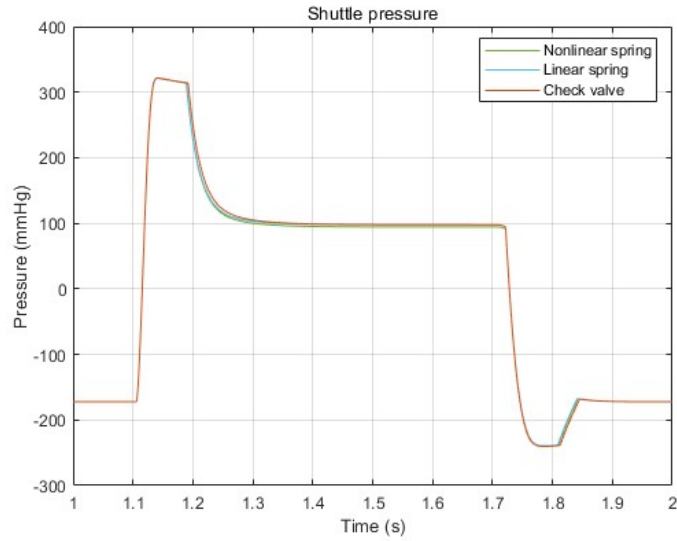


Figure 5.6: Shuttle pressure at its best case scenario, when all three models show overall similar results. Green represents the nonlinear spring-damper system, blue the linear spring-damper system and red the check valve approach.

At 50 mmHg, the three models produce very similar shuttle pressure waveforms, which can be seen in Figure 5.6. This indicates that the sensitivity to the internal balloon law under these conditions is limited.

Effect of chamber pressure on inflation plateau. Across different chamber pressures, the end-of-inflation plateau differs depending on the model.

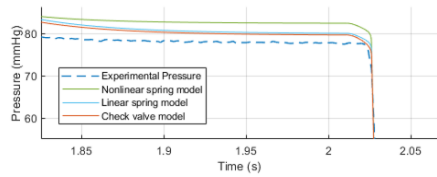


Figure 5.7: End-of-inflation shuttle pressure at 25 mmHg chamber pressure.

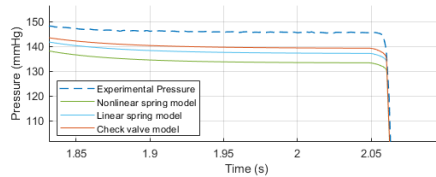


Figure 5.8: End-of-inflation pressure at 100 mmHg chamber pressure.

Figures 5.7 and 5.8 show the end of inflation plateau for the different models over different environmental pressures. The check valve approach is closest to the measured plateau.

Error metrics. To summarize performance, the root mean square error (RMSE) over time was computed over three heart beats for shuttle pressure and chamber pressure. The absolute plateau error at end inflation was also calculated.

All errors are presented in mmHg and are averaged across the nine test cases per model, described in Section 4.5.2:

Model	RMSE Shuttle P	RMSE Env P	Plateau diff
Check valve	11.82	1.70	3.11
Linear spring	14.08	1.87	4.02
Nonlinear spring	14.19	1.85	5.47

Table 5.1: Average errors across models ($n = 9$ per model). Shuttle P and Env P represent the errors in shuttle gas pressure and environmental pressure, and Plateau diff the plateau error at end inflation.

Table 5.1 shows errors across the three models, with the check valve approach yielding the lowest shuttle pressure RMSE and smallest plateau error on average.

5.3 Use case results: Altitude test

This use case evaluated performance across atmospheric pressure and heart rates. All altitude test results use the check valve balloon model, selected since it best matched experimental plateaus and had the lowest RMSE, see Table 5.1. The 10-90 % inflation and deflation times are shown, as well as the full inflation volume.

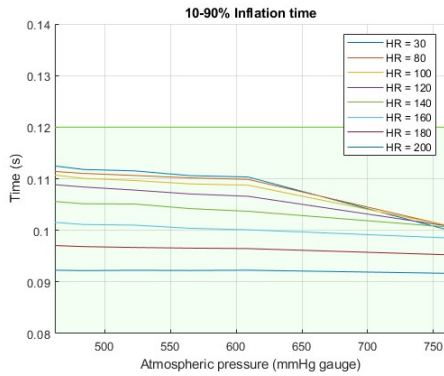


Figure 5.9: Inflation 10-90 % time vs atmospheric pressure. Each curve corresponds to a different heart rate (bpm). The requirement is ≤ 0.12 s.

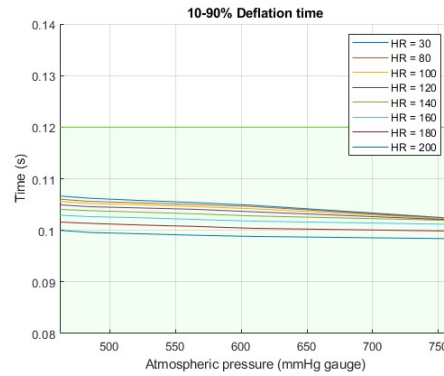


Figure 5.10: Deflation 10-90 % time vs atmospheric pressure. Each curve corresponds to a different heart rate (bpm). Requirement: ≤ 0.12 s.

Across the tests, inflation and deflation times decrease with altitude, and decrease when heart rate increases. This can be seen in Figures 5.9 and 5.10. For all combinations, both metrics remain within the ≤ 0.12 s requirement. Deflation times are similar to inflation times over all conditions.

The full inflation volume for the different tests can be seen below:

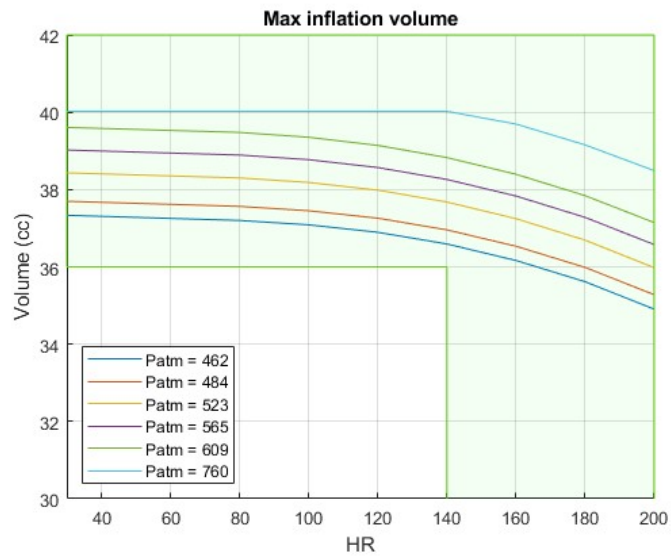


Figure 5.11: Balloon volume at full inflation, with each line representing a different atmospheric pressure. The green area is the range for acceptable results.

Figure 5.11 shows that maximum inflation volume varies with atmospheric pressure and heart rate (HR) but remains within the specified acceptance range. For higher heart rates, a lower full inflation volume is allowed, which is shown in the green area.

6 Discussion

6.1 Compressor

In this project, the pressure and vacuum reservoirs are maintained using a **Positive-Displacement Compressor (G)** block driven by a tabulated motor speed. While the compressor block yields reasonable results for the pressure in the reservoirs, it fails to match the experimental compressor behavior even at atmospheric pressure. At sea level, the block reproduces the behavior of the IABP, the vacuum reservoir pressure is pulled down after each deflation and the pressure reservoir is restored. However, performance degrades as atmospheric pressure changes. There can be several reasons affecting this, outlined below.

Pressure-ratio sensitivity. The block computes mass flow from displacement, speed and inlet specific volume:

$$\dot{m} = \eta_v \omega \frac{V_{disp}}{V_s}. \quad (64)$$

If η_v is not provided as a map that depends on pressure ratio as well as speed, the model cannot capture how different properties affect the volumetric efficiency at different pressure ratios. Therefore, tuning only at sea level does not generalize well to other atmospheric pressures.

Temperature effects. Temperature effects in the model might also be under-modeled. Temperature in the compressor influences the mass flow rate only through the inlet specific volume V_s , which uses nominal conditions. The block does not use temperature dependent efficiency maps, and as a result gas temperature is not represented realistically.

Speed law simplification. The motor speed is approximated by a static, heart rate based table, see Table 3.1. The real device regulates speed in closed loop based on pressure levels. The simplification in this model is an aspect that affects the results.

Potential upgrades. To improve realism in the model, some upgrades could be considered:

- Adding efficiency maps to better capture volumetric efficiency dynamics. For this, more experiments or data is needed.
- Custom build compressor. A custom compressor could be built either using a custom Simscape component or by dividing the compressor into several parts.
- Implement control system. Replace the tabulated RPM values with a simple PID controller could potentially capture the devices regulation dynamics and reduce mismatch in results even if the compressor physics remain simplified.

In short, the current Positive-Displacement Compressor works for sea-level, nominal pressure ratio scenarios but lacks the temperature and pressure ratio dependencies needed for capturing behavior over multiple altitudes.

6.2 Resistance

It was hypothesized that the missing resistance in the shuttle gas flow might vary with external pressure. However, by having a constant flow restriction over the different environmental pressures, this produced realistic behavior across the different simulations. This suggests that, within the range of pressures tested in the experiments, the believed pressure-dependent changes in resistance were either negligible or effectively compensated by the restriction.

If we use equation (7) and calculate the resistance over the catheter in the model, and the local restriction, we get the following plot:

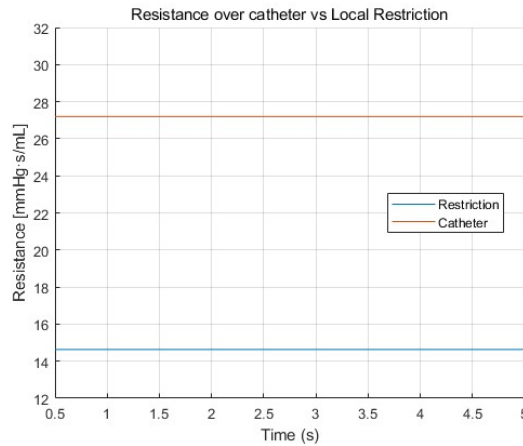


Figure 6.1: Comparison of resistance over catheter and local restriction.

Looking at Figure 6.1, it can be seen that the catheter remains the dominant contributor to the resistance in the system. The local restriction acts as a small corrective pressure drop that likely stands in for unmodeled minor losses such as connectors, bends, balloon entrance effects or other practical details not captured by the current model.

Physically motivating the extra pressure drop with a single local restriction is difficult. As mentioned in Section 3.3.4, minor losses from bends and fittings can be modeled via equivalent lengths, which were neglected here while the previous model overstated them, which could be a cause for the need of a small lumped restriction. A way to increase realism is to reintroduce minor loss elements using tabulated equivalent lengths specific for the tubing fittings, if available.

Overall, the results indicate that the catheter drives most of the resistance while a small lumped restriction is sufficient to model the remaining pressure losses across the different conditions.

6.3 Balloon models

Across the three balloon models, the overall cycle dynamics are broadly similar. The check valve model, however, reproduces the inflation plateau more consistently over different chamber pressured, which reduces estimation error and improves robustness.

Check valve model benefits. As discussed in Section 3.4.2, the balloon exhibits a threshold, or valving, behavior. This can also be enhanced by the balloon collapsing at its entrance due to hydrostatic effects, causing further valving effects at deflation. Implementing check valves with a cracking pressure and a full-open threshold mimics this effect. In practice, the inflation pressure rises quickly, so the threshold is crossed early in the cycle, which is why large differences between the models are not always visible.

6.4 Valve dynamics

If we look closer at the shuttle pressure in Figure 5.5, and zoom in on one of the inflation peaks, we see that the rise in pressure is more sharp than the experimental results:

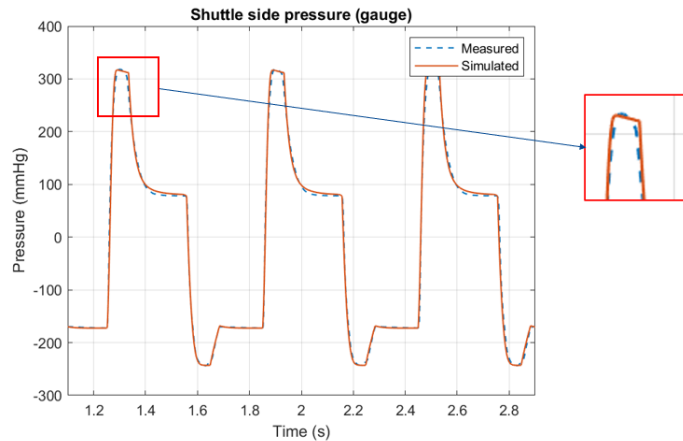


Figure 6.2: Shuttle pressure, for environmental pressure 50 mmHg and a heart rate of 80 bpm. Experimental results shown in dotted blue and Simscape results in red.

Figure 6.2 shows that the simulated shuttle pressure upstroke is sharper than that of the measured one, and the plateau does not fully settle before deflation. In the model the pressure valve opens almost instantaneously, while the real valve might have slower dynamics, affecting the upstroke. The model triggers inflation and deflation from a heart-rate schedule, where the real device use ECG/aortic pressure to trigger the cycles. This could lead to phase errors, and cannot capture variation between heart beats. Additionally, the output signal from the CardioSave measurements is filtered or averaged, leading to a smoother appearance in the measured data. These factors make it challenging to directly

know the exact reason for the differences between the experimental data and simulated results.

The observed variation of the inflation plateau with chamber pressure suggests that one or more model parameter maybe should depend on transmural pressure. In the present model, the cracking and full-open thresholds of the balloon check valves, the added local restriction and the balloon compliance are constant. In reality, the entry restriction and other parameters might change with higher environmental pressure.

6.5 Parameter estimation

It can be seen when looking at the figures from the altitude tests, Figure 5.10 and 5.9, that the model yields similar inflation and deflation times, and occasionally a shorter deflation time. This contradicts observations, where usually the deflation is slower. One possible explanation is that the parameter estimation in this project is tailored to the specific experimental setup, potentially leading to parameter values that do not generalize well. Additional parameter tuning might be required to obtain more accurate and realistic model behavior.

6.6 Numerical method

The Simscape network yields a stiff, index-1 DAE with fast transients such as valve events. An implicit, variable-step scheme is therefore appropriate, and in this work `daessc` was used, which is based on a second-order numerical differentiation formula (NDF2).

The modified equation analysis in (63) shows an $O(\Delta t^2)v'''$ perturbation containing only odd derivatives. This indicated numerical dispersion (phase error) rather than dissipation, sharp features propagate with a slightly altered phase speed while amplitudes are largely preserved. Consistent with this, the simulated pressure in Figures 5.1 and 5.2 show a small phase lag at the steep fronts.

The leading error scales like Δt^2 , which means that tightening the step size near rapid events might reduce the phase error.

7 Conclusions and future Work

7.1 Conclusions

This work developed a lumped-parameter Simscape model of the intra-aortic balloon pump (IABP) that reproduces the major pneumatic dynamics observed from experiments. The model captures the timing and magnitude of shuttle side inflation and deflation cycles and the regulation behavior of the vacuum reservoir across a range of test conditions.

Three balloon representations were evaluated (nonlinear spring, linear spring, and a soft linear spring with check valves). All produced similar cycle shapes, but the check valve approach yielded the most consistent inflation plateau across environmental pressures and the lowest aggregate error, with the RMSE being 11.8 mmHg compared to 14.1-14.2 mmHg for the spring models, see Table 5.1. This supports the hypothesis that a threshold-like valving effect is present in practice and is advantageous to include in the model.

The altitude test use case demonstrates the model's usefulness. Simulated inflation/deflation 10–90 % times remained within the 0.12 s requirement over the tested heart rates and atmospheric pressures, and full-inflation volumes stayed within limits. This illustrates how the model can be useful when trying out new algorithms when developing the device, before testing in a lab environment.

While the compressor model does not reproduce the measured LPM–RPM curve or pressure-ratio dependence, the simplified model still maintains the reservoirs at correct pressures for nominal conditions. Driving the compressor with a heart-rate based speed table provides a workable simplification for the device's closed-loop controller, however, it lacks the ability to handle beat-to-beat variation and cannot capture the fine speed adjustments observed in the device.

7.2 Future work

To further develop the model and improve realism, a few points of future work are suggested:

- Valve modeling. Replace the current approximations with parameters from real data from the device. Collect more data and model the valves more close to reality.
- Signal-driven triggering. Allow the model to accept clinical triggers such as aortic pressure or ECG, so that inflation and deflation timing matches practice and reduces phase errors in triggering.
- Compressor. Calibrate the compressor with additional data over different pressure ratios or switch to a component level compressor model that includes thermal effects.
- Patient coupling. Couple to a cardiovascular model to be able to see direct hemodynamic impact of device-side changes.

References

- [1] *A century and beyond with Getinge in medtech - Getinge*. URL: <https://www.getinge.com/int/company/news/press-releases/2024/4779076-A-century-and-beyond-with-Getinge-in-medtech/> (visited on 06/02/2025).
- [2] Abdolrazaghi, Mona, Navidbakhsh, Mahdi, and Hassani, Kamran. "Mathematical modelling of intra-aortic balloon pump". In: *Computer Methods in Biomechanics and Biomedical Engineering* 13.5 (Oct. 2010), pp. 567–576. ISSN: 1025-5842, 1476-8259. DOI: 10.1080/10255840903352532. URL: <http://www.tandfonline.com/doi/abs/10.1080/10255840903352532>.
- [3] Bogacki, P. and Shampine, L.F. "A 3(2) pair of Runge - Kutta formulas". In: *Applied Mathematics Letters* 2.4 (1989), pp. 321–325. ISSN: 08939659. DOI: 10.1016/0893-9659(89)90079-7. URL: <https://linkinghub.elsevier.com/retrieve/pii/0893965989900797>.
- [4] Brenan, Kathryn E., Campbell, Stephen L., and Petzold, Linda Ruth. *Numerical solution of initial-value problems in differential-algebraic equations*. Unabridged, corr. republ., New York, 1989. Classics in applied mathematics 14. Philadelphia, Pa: SIAM, 1996. 256 pp. ISBN: 978-0-89871-353-4.
- [5] *Congestive Heart Failure: What Does It Mean?* Cleveland Clinic. URL: <https://my.clevelandclinic.org/health/diseases/17069-heart-failure-understanding-heart-failure> (visited on 04/19/2025).
- [6] De Lazzari, Claudio et al. "Intra-aortic balloon counterpulsation timing: A new numerical model for programming and training in the clinical environment." In: *Computer Methods and Programs in Biomedicine* 194 (Oct. 2020), p. 105537. ISSN: 01692607. DOI: 10.1016/j.cmpb.2020.105537. URL: <https://linkinghub.elsevier.com/retrieve/pii/S0169260720308257>.
- [7] *Do You Know Where Your Femoral Artery Is?* Cleveland Clinic. URL: <https://my.clevelandclinic.org/health/body/21645-femoral-artery> (visited on 04/20/2025).
- [8] *Dormand-Prince method*. In: *Wikipedia*. Page Version ID: 1279549582. Mar. 9, 2025. URL: https://en.wikipedia.org/w/index.php?title=Dormand%E2%80%93Prince_method&oldid=1279549582 (visited on 04/15/2025).
- [9] Institute, National Heart Lung {and} Blood. *Heart valves NIH*. Nov. 12, 2013. URL: https://commons.wikimedia.org/wiki/File:Heart_valves_NIH.jpg (visited on 05/13/2025).

- [10] *Intraaortic_Balloon.png (1956×1468)*. URL: https://commons.wikimedia.org/wiki/File:Intraaortic_Balloon.png (visited on 05/27/2025).
- [11] *Intraoperative intra-aortic balloon pump insertion: step by step*. MMCTS. URL: <https://mmcts.org/tutorial/1942> (visited on 04/12/2025).
- [12] Kantrowitz, Adrian et al. “Initial Clinical Experience With Intraaortic Balloon Pumping in Cardiogenic Shock”. In: *JAMA* 203.2 (Jan. 8, 1968), pp. 113–118. ISSN: 0098-7484. DOI: 10.1001/jama.1968.03140020041011. URL: <https://doi.org/10.1001/jama.1968.03140020041011>.
- [13] Khan, Tahir M. and Siddiqui, Abdul H. “Intra-Aortic Balloon Pump”. In: *StatPearls*. Treasure Island (FL): StatPearls Publishing, 2025. URL: <http://www.ncbi.nlm.nih.gov/books/NBK542233/>.
- [14] Klopfenstein, R.W. “Numerical differentiation formulas for stiff systems of ordinary differential equations”. In: *RCA Review* 32 (1971), pp. 447–462.
- [15] Merritt, David and Weinhaus, F. “The pressure curve for a rubber balloon”. In: *American Journal of Physics* 46 (Oct. 1978), pp. 976–977. DOI: 10.1119/1.11486.
- [16] Mouloupoulos, Spyridon D., Topaz, Stephen, and Kolff, Willem J. “Diastolic balloon pumping (with carbon dioxide) in the aorta—A mechanical assistance to the failing circulation”. In: *American Heart Journal* 63.5 (May 1, 1962), pp. 669–675. ISSN: 0002-8703. DOI: 10.1016/0002-8703(62)90012-1. URL: <https://www.sciencedirect.com/science/article/pii/0002870362900121>.
- [17] Niederer, P. and Schilt, W. “Experimental and theoretical modelling of intra-aortic balloon pump operation”. In: *Medical and Biological Engineering and Computing* 26.2 (Mar. 1, 1988), pp. 167–174. ISSN: 1741-0444. DOI: 10.1007/BF02442260. URL: <https://doi.org/10.1007/BF02442260>.
- [18] Ojha, Niranjan and Dhamoon, Amit S. “Myocardial Infarction”. In: *StatPearls*. Treasure Island (FL): StatPearls Publishing, 2025. URL: <http://www.ncbi.nlm.nih.gov/books/NBK537076/> (visited on 04/19/2025).
- [19] Parissis, H. et al. “IABP: history-evolution-pathophysiology-indications: what we need to know”. In: *Journal of Cardiothoracic Surgery* 11.1 (Aug. 4, 2016), p. 122. ISSN: 1749-8090. DOI: 10.1186/s13019-016-0513-0. URL: <https://doi.org/10.1186/s13019-016-0513-0>.
- [20] Ragosta, Michael and Kennedy, Jamie. “Normal Waveforms, Artifacts, and Pitfalls”. In: Jan. 2018, pp. 17–55. ISBN: 9780323480420. DOI: 10.1016/B978-0-323-48042-0.00002-6.

- [21] Rohani, C. et al. “Mortality in patients with myocardial infarction and potential risk factors: A five-year data analysis”. In: *ARYA Atherosclerosis* 18.3 (May 2022), pp. 1–8. DOI: 10.48305/arya.v18i0.2427.
- [22] Shampine, Lawrence F. and Reichelt, Mark W. “The MATLAB ODE Suite”. In: *SIAM Journal on Scientific Computing* 18.1 (Jan. 1997), pp. 1–22. ISSN: 1064-8275, 1095-7197. DOI: 10.1137/S1064827594276424. URL: <http://epubs.siam.org/doi/10.1137/S1064827594276424>.
- [23] Swift, Hilary and Bordoni, Bruno. “Anatomy, Bony Pelvis and Lower Limb: Femoral Artery”. In: *StatPearls*. Treasure Island (FL): StatPearls Publishing, 2025. URL: <http://www.ncbi.nlm.nih.gov/books/NBK538262/> (visited on 04/20/2025).
- [24] The MathWorks, Inc. *Optimization Toolbox*. MathWorks. 2024. URL: <https://se.mathworks.com/products/optimization.html>.
- [25] The MathWorks, Inc. *Simscape*. MathWorks. 2024. URL: <https://se.mathworks.com/products/simscape.html>.
- [26] Thin Pa Pa Aye and Naiyanetr, Phornphop. “Modelling and simulation of cardiovascular system with intra-aortic balloon pump”. In: *The 6th 2013 Biomedical Engineering International Conference*. 2013 6th Biomedical Engineering International Conference (BMEiCON). Amphur Muang, Krabi, Thailand: IEEE, Oct. 2013, pp. 1–4. ISBN: 978-1-4799-1467-8 978-1-4799-1466-1. DOI: 10.1109/BMEiCon.2013.6687728. URL: <http://ieeexplore.ieee.org/document/6687728/>.
- [27] Westerhof, Nico, Lankhaar, Jean-Paul, and Westerhof, Berend E. “The arterial Windkessel”. In: *Medical & Biological Engineering & Computing* 47.2 (2009), pp. 131–141. DOI: 10.1007/s11517-008-0359-2.
- [28] Westerhof, Nico et al. “Law of Poiseuille”. In: *Snapshots of Hemodynamics*. Springer, Cham, 2019. ISBN: 978-3-319-91931-7. DOI: 10.1007/978-3-319-91932-4_2. URL: https://doi.org/10.1007/978-3-319-91932-4_2.
- [29] *What is the ideal gas law? (article) | Gases*. Khan Academy. URL: <https://www.khanacademy.org/science/physics/thermodynamics/temperature/a/what-is-the-ideal-gas-law> (visited on 04/19/2025).
- [30] Wikimedia Commons. *Davvisámegiella: Olbmo váibmu*. Jan. 10, 2020. URL: https://commons.wikimedia.org/wiki/File:Diagram_of_the_human_heart_se.svg#/media/File:Diagram_of_the_human_heart.svg (visited on 04/14/2025).

- [31] World Health Organization. *Cardiovascular diseases (CVDs)*. Accessed: 2025-08-10. 2025. URL: https://www.who.int/health-topics/cardiovascular-diseases#tab=tab_1.
- [32] Zewde Hägglund, M. “Pneumatic Model of Intra Aortic Balloon Pump”. Master’s thesis. KTH Royal Institute of Technology, 2025. URL: <https://urn.kb.se/resolve?urn=urn:nbn:se:kth:diva-361509>.

TRITA-SCI-GRU 2025-525
Stockholm, Sweden 2025

www.kth.se